

ARTICLE OPEN



Insights into the mechanisms controlling the residual corrosion rate of borosilicate glasses

Stephane Gin¹, Xiaolei Guo², Jean-Marc Delaye¹, Frédéric Angeli¹, Kamallesh Damodaran¹, Véronique Testud³, Jincheng Du⁴, Sebastien Kerisit⁵ and Seong H. Kim⁶

Borosilicate glasses are widely used to confine high-level radioactive wastes. The lifetime of these materials could reach hundreds of thousands of years if leaching of the glass into groundwater enables the formation of a passivating gel layer. Even in this regime, the glass will never stop corroding as thermodynamic equilibrium between glass and solution cannot be achieved. Therefore, accurate predictions of glass durability including passivation, require a deep understanding of the mechanisms controlling the so-called residual rate. However, despite tremendous efforts, these mechanisms remain poorly understood. Here, focusing on the behavior of the soluble elements of the International Simple Glass (B, Na, and Ca), we show that the residual rate is controlled by the behavior of B, a glass former supposed to dissolve instantaneously when in contact with water and thus widely considered as an ideal tracer. We then demonstrate that B release is controlled by multiple processes highly dependent on the pH. At the beginning of the passivating layer formation, the hydrolysis of B-O-Si linkages is rate-limiting and has an activation energy of $\sim 60 \text{ kJ mol}^{-1}$, a value slightly lower than that for breaking Si-O-Si linkages. Once the fraction of closed pores resulting from gel restructuring is high enough, then diffusion of both reactants (water molecules) and some products (mainly B_{aq} , Ca_{aq}) through the growing gel layer becomes rate-limiting. Consequently, B and Ca accumulate in an inner layer referred to as the active zone, with potential feedback on the B-O-Si hydrolysis. A new paradigm, including B as a key element of the system, is proposed to develop a comprehensive model for the corrosion of borosilicate glass.

npj Materials Degradation (2020)4:41 ; <https://doi.org/10.1038/s41529-020-00145-2>

INTRODUCTION

For decades, borosilicate glasses have been designed to immobilize high-level radioactive waste produced in nuclear power plants¹. The United States, France, Japan, the United Kingdom, and Germany, among others, have produced thousands of metric tons of nuclear waste glass, and then poured in stainless steel canisters, while being cooled, to dispose of them in a geological repository². Owing to the presence of long-lived fission products and minor actinides, the typical time scale for the safety demonstration of such disposals is ~ 1 million years^{1,3}. Repository developers have adopted a multi-barrier, defense-in-depth approach in which the primary barrier is the glass waste form itself⁴. But groundwater is expected to infiltrate the repositories, causing glass to corrode^{5,6}. Depending on temperature (25–90 °C) as well as solution and glass composition, corrosion rates of nuclear waste glasses can vary over 4 to 6 orders of magnitude (from a few $\mu\text{m}/\text{day}$ for the initial dissolution rate measured in dilute solutions to a few nm/year for the residual rate measured in silica saturated solution). A low temperature, Si-rich solutions with $\text{pH}_{25^\circ\text{C}}$ between 9 and 10 lead to extremely low corrosion rates⁷, which are expected to translate to glass package lifetime on the order of 10^5 – 10^6 years. However, despite being arguably the most important glass corrosion regime, the residual rate regime remains poorly understood and glass scientists are unable to accurately predict glass durability in the passivation regime^{8,9}.

In 1984, Grambow hypothesized that corrosion of silicate glasses never stops because of the metastable nature of the material¹⁰. As a result, and unlike minerals, once saturation with

respect to the silicate matrix is achieved in the surrounding solution phase, glass continues to corrode at a low, residual rate potentially controlled by glass hydration and subsequent release of soluble elements (mainly alkali and boron). A general rate law was derived from this idea along with concepts arising from transition state theory (TST)¹¹:

$$r = r_0 \left(1 - \frac{[\text{H}_4\text{SiO}_4]}{K} \right) + r_r \quad (1)$$

where r is the glass corrosion rate, r_0 is the initial (or forward) dissolution rate, $[\text{H}_4\text{SiO}_4]$ is the activity of orthosilicic acid at the glass surface, K is the equilibrium constant (which equals the activity of orthosilicic acid at saturation) and r_r is a constant term standing for the residual rate. The corrosion rate, r , corresponds to the time dependence of the transformation of the pristine glass into dissolved species plus alteration products (gel, secondary phases), which can be monitored either by the progress of the hydration front into the glass, or the release of mobile glass cations in the bulk solution. Boron or sodium are typically used as the corrosion tracer because of their high solubility and low retention in the alteration products. In Grambow's approach, because hydrolysis reactions take place in series regardless of the complexity of the glass, the whole corrosion process is predicted to be controlled by its slowest elementary reaction. Grambow then theorized that, for borosilicate glasses used as containment matrices for nuclear waste, the rate-limiting reaction was the breaking of the fourth bond linking a SiO_4 tetrahedron to the silicate network to form an aqueous silicate species, which led to

¹CEA, DES, ISEC, DE2D, University of Montpellier, Marcoule, F-30207 Bagnols sur Cèze, Montpellier, France. ²Department of Materials Science and Engineering, Ohio State University, Columbus, OH 43210, USA. ³CEA, DES, ISEC, DMRC, University of Montpellier, Marcoule, F-30207 Bagnols sur Cèze, Montpellier, France. ⁴Department of Materials Science and Engineering, University of North Texas, Denton, TX 76203, USA. ⁵Physical Sciences Division, Pacific Northwest National Laboratory, Richland, WA 99354, USA. ⁶Department of Chemical Engineering and Materials Research Institute, Pennsylvania State University, University Park, PA 16802, USA. ✉email: stephane.gin@cea.fr

the simple first-order affinity term in Eq. 1¹². Regardless of the robustness of the theoretical foundations of this law, it is a fact that most of the kinetic models developed to date have inherited the affinity term from Grambow's pioneering work^{13–19}. Since then, it has come to light that the gel formed by condensation of partially or totally detached species from the glass surface can limit transport, and that dissolved glass components other than Si must be considered in the affinity term^{9,20,21}. An apparent diffusion coefficient for one or several species was considered to globally account for the phenomenon of passivation^{13–15,22,23}. However, the fundamental reason why glass still corrodes once the affinity term vanishes and the mechanisms that control this residual rate have remained elusive. Beyond Grambow's hypothesis relying on hydration²⁴, several other individual or coupled possible rate-controlling mechanisms have been evaluated, such as ion-exchange^{24–26}, precipitation of secondary phases²⁶, gel dissolution¹⁴, and diffusion of water²⁷, silicon²⁴ or tracing elements²² through the gel, but no definitive demonstration has been made. Consequently, no model is currently comprehensive enough to accurately predict the residual rate of a given glass corroded in a given set of experimental conditions. Several reasons account for this profusion of hypotheses: (i) many intrinsic and extrinsic factors affect glass behavior (composition and structure of the glass, temperature, pH, solution composition, and radioactivity), which make the development of a unified approach challenging, (ii) residual rates are generally extremely low, resulting in small amounts of alteration products, which, in turn, make detailed characterizations difficult, and, last but not least, (iii) the discovery of a correlation does not imply that the root causes have been identified.

To bring to light the mechanisms that control the residual rate, we performed extensive characterization of samples of the International Simple Glass (ISG)—a 6-oxide aluminoborosilicate glass used as a reference by the glass corrosion community²⁸—corroded for 6 years at pH 7 or 9 in a silica-saturated solution (i.e., $r = r_r$ according to Eq. 1). These samples are of great interest because their r_r differ by approximately a factor of 6, i.e., $r_r(\text{pH}7) = \sim 6 \cdot r_r(\text{pH}9)$ ^{29,30}. The gels formed in these experiments have been deeply investigated at different stages of the reaction^{27,29–34}, and more samples are still under corrosion and thus available for further investigations. Previous characterizations concluded that the gel composition, pore volume, pore size, and structure are similar at pH 7 and pH 9, only their thickness differs significantly (by a factor ~ 6)^{27,29–34}. The origin of this difference remained unclear because it is opposite to what is observed in dilute conditions³⁵. It was then thought that addressing this question would improve the understanding of the rate-limiting mechanisms of the residual rate. This study consists of three complementary experiments. In *Experiment 1*, we compared the time-dependent composition of gels formed at pH 7 and 9. In *Experiment 2*, we analyzed the glass response following a pH change (coupons corroded for 6 years at pH 9 were put in solutions at pH 3, 5, or 7, respectively). Time-of-flight secondary ion mass spectrometry (ToF-SIMS) and inductively coupled plasma mass spectrometry (ICP-MS) were employed to analyze the altered coupons and the leaching solutions after the change in pH, respectively. To support the interpretation of the results, *Experiment 3* was conducted with pristine glass specimens to parameterize the release rate of B as a function of pH and temperature. The results of these three experiments collectively prove that the status of B as an ideal corrosion tracer must be reconsidered. Furthermore, we demonstrate that the residual rate is governed by the coupled effects of slow diffusion through the growing gel and pH-dependent hydrolysis reactions within a reactive interfacial region.

RESULTS

Experiment 1

In the conditions of *Experiment 1* (static, 90 °C, Si-saturated solution, pH 7 or 9), glass corrodes at a constant volume and no secondary minerals precipitate. This means that corrosion transforms a given volume of glass into the same volume of gel^{29,32}. In Fig. 1, the time evolution of the gel thickness is determined from B and H ToF-SIMS depth profiling (Fig. 1a–d and Supplementary Figs. 1–2) and from B concentrations in the leachate (Fig. 1e). The two datasets are consistent and indicate that, in both tests, ISG starts corroding at a high rate, which then drops markedly after a few weeks, and eventually becomes nearly constant. This is in agreement with previous studies, which demonstrated that the gel must grow and mature/reorganize before it significantly impacts the rate^{27,36–38}. In the following, the term residual rate refers to the near-constant rate after the passivating gel is formed (typically between 200 and 2000 days in *Experiment 1*). Hence, r_r equals $0.2 \pm 0.1 \text{ nm} \cdot \text{d}^{-1}$ at pH 7, based on both solution and SIMS data. The value derived from B concentration is slightly underestimated as some B is retained in the gel (Fig. 1a). However, by combining data displayed in Supplementary Figs. 1, 2 it can be calculated that the mean retention factor of B in the gels formed at pH 7 is around 12%, which implies that the rate is underestimated by $100/(1 - 0.12) = 14\%$, a value which remains within uncertainties. The value of r_r at pH 9 equals $0.03 \pm 0.02 \text{ nm} \cdot \text{d}^{-1}$, based on SIMS data only. It is worth noting that the samplings were highly diluted prior to their analysis by ICP-OES because of the high concentration of K in the leachates. Moreover, *Experiment 1* was conducted at low glass-surface-area to solution-volume ratio (S/V) which implies a low concentration of glass components in the leachate. Consequently, variations of B concentration over time remained within uncertainties for the test at pH 9 and r_r could not be calculated from these data. Although the value of r_r at pH 9 is given with a large uncertainty, it is close to that reported from a 14-year long experiment with glass powder and no K in the leaching solution ($0.06 \pm 0.02 \text{ nm} \cdot \text{d}^{-1}$)³⁹.

Globally, B and H profiles recorded in corroded samples from *Experiment 1* are anti-correlated and display a sharp interface between the gel and the pristine glass. Nonetheless, looking closely at those profiles, 3 sublayers can be distinguished (Fig. 2). Note that all depth profiles of the samples from *Experiment 1* can be processed the same way. From the pristine glass toward the solution, a first layer, referred to as the *hydrated glass* (HG), is delineated by the H front and the inner B front, which is given by a normalized concentration of B, $C(B)$, of 0.5 (half-height of the sharp gradient between the pristine glass and the gel layer); a second layer, called *active zone* (AZ), is comprised between the inner and outer B fronts at $C(B) = 0.5$ and $C(B) = 0.2$, respectively; and a third layer, the *bulk gel* (BG), is delineated by $C(B) = 0.2$ and the outer surface of the gel. The position of the outer layer of the AZ at $C(B) = 0.2$ corresponds to the transition observed on all the samples from *Experiment 1* between the sharp interfacial gradient and the low concentration gradient, when it exists (durations > 7 days). Importantly, defining the front positions based on Ca rather than B would lead to the same results. With Na, results might be slightly different, mainly because Na is less retained in the gel than B and Ca. A previous study showed that B and Na dissolve congruently at pH 4, a pH value that favors Na^+/H^+ exchange³⁵. As Na is less energetically bonded to the glass network than B, and thus more prone to undergo hydrolysis, the behavior of B, Na, and Ca in our experiments implies that the dissolution of B likely limits that of Na and Ca. It is reminded that, in previous studies, a thin outermost precipitated layer with a thickness of $\sim 10 \text{ nm}$ was identified based on its isotopic signature being close to that of the solution^{29,30}. This layer was not considered in the following analysis because it forms at the very beginning of the reaction and does not evolve over time; thus, it is not a diffusion barrier²⁹. The

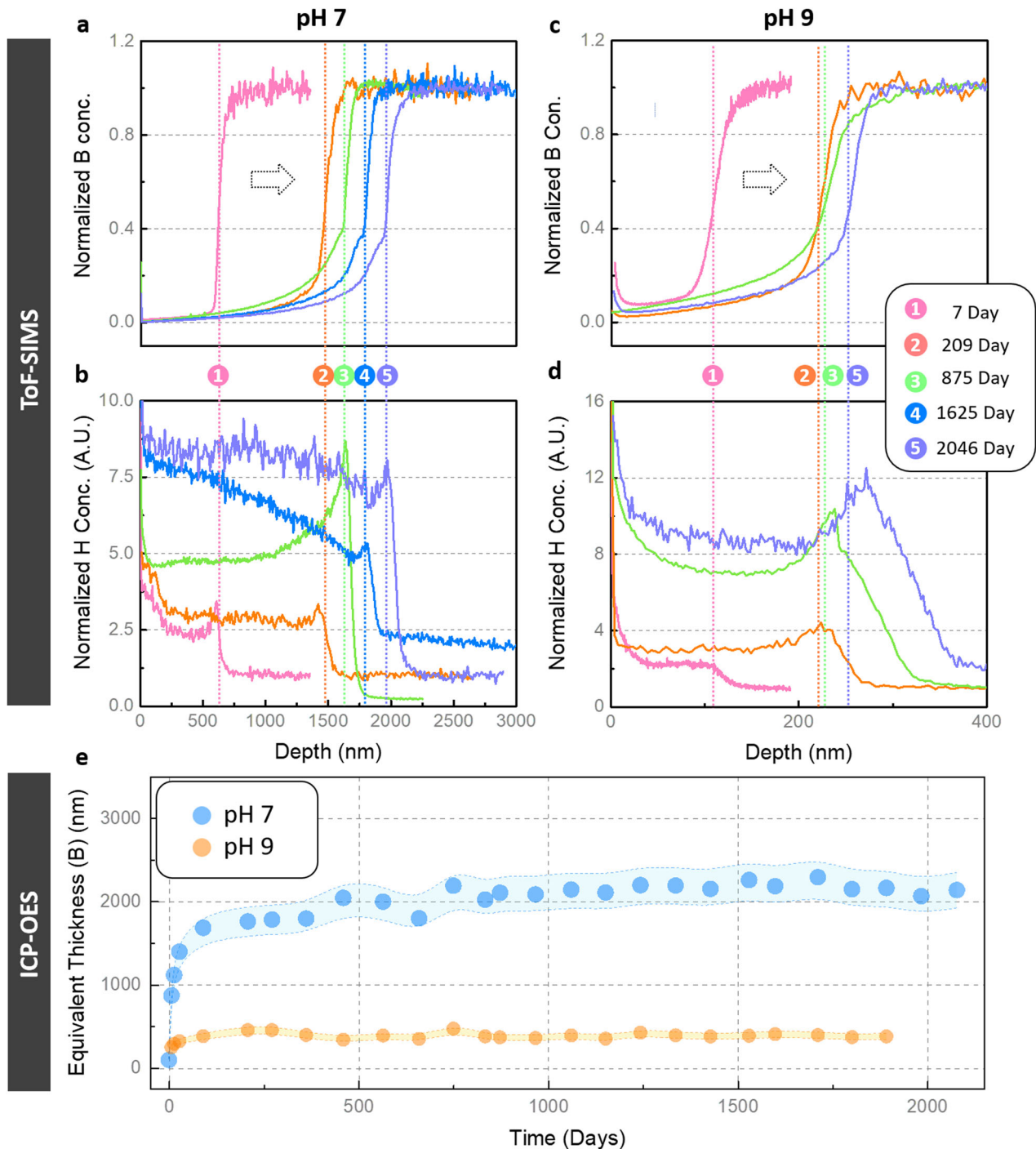


Fig. 1 Solid and solution data from Experiment 1 conducted with ISG specimens corroded at 90 °C in a silica-saturated solution at pH 7 or 9. **a, b** ToF-SIMS profiles of B and H at various durations for the test conducted at pH 7. For B, intensities were normalized to that of Zr, an immobile element, and the resulting ratio was normalized to the mean value of B/Zr in the pristine glass. Therefore, B data are quantitative whereas H data are qualitative. **c, d** Same as a-b for the test conducted at pH 9. In **a–d**, vertical dashed lines are placed at $C(B) = 0.5$ (boundary between the bulk gel and the active zone). The shift of the H front with time is clearly visible at pH 9. **e** Gel thickness calculated from B release in solution.

HG layer displays anti-correlated H/Na profiles characteristic of ion-exchange reactions⁴² and a moderate depletion in B and Ca. The AZ is characterized by a H peak, the absence of Na, and intermediate retention factors for B and Ca. The BG has a near-constant composition with a low retention factor for the mobile glass cations. This delineation matches the textural analysis of the gels performed by spectroscopic ellipsometry and water adsorption isotherms, showing a porosity increasing with the

replacement of mobile glass cations by hydrous species³¹. Here, we show that the concentrations of B, Na, and Ca are low and constant over time in the BG whereas they are higher and time-dependent in the other two layers (Supplementary Fig. 1). B and Ca tend to accumulate in the AZ and HG whereas these layers are depleted in Na. Additionally, the growth rate of each layer decreases following BG > AZ > HG (Supplementary Figs. 2-3). Therefore, most of the B released into the bulk solution comes

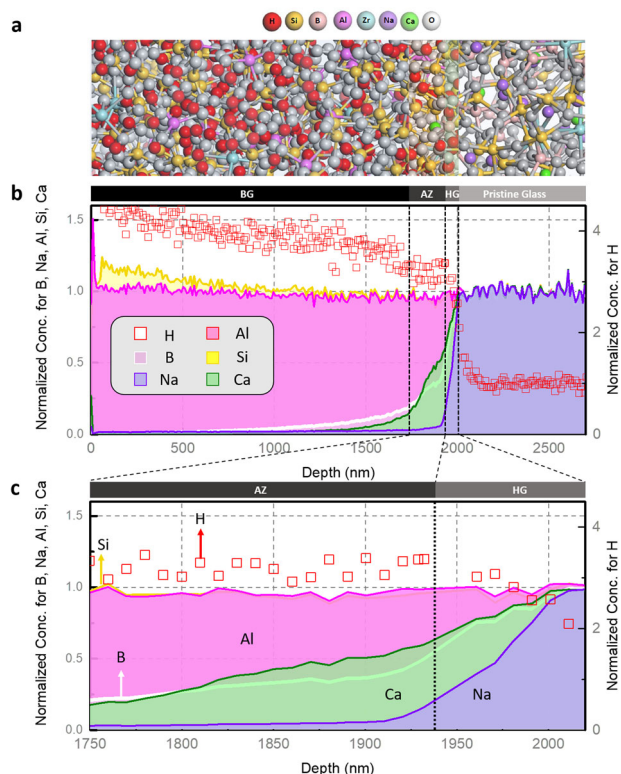


Fig. 2 Identification of the various sublayers within the gel-hydrated glass (HG), active zone (AZ), bulk gel (BG). For glass cations i , intensities are normalized to that of Zr, an immobile element, and the resulting ratio is normalized to the mean value of i/Zr in the pristine glass. For H, intensities are normalized to the mean value in the pristine glass. Therefore data for glass cations are quantitative whereas they are only qualitative for H. **a** Snapshot of the various layers characterized by their compositions from ISG structural model generated from molecular dynamics simulations³². **b** Elemental profiles obtained for the sample pH 7 - 2312 days. **c** Zoomed-in view of the interfacial area with details of the HG and AZ. The interfacial gradient can result from either a real chemical gradient or a rough interface^{30,40,41}.

from the transformation of the AZ into BG. Based on this analysis, we hypothesize that the dissolution of B within the AZ and the diffusion of dissolved species through the gel are the rate-limiting mechanisms controlling the ISG residual rate in the tested conditions. It is worth noting that the key role of the AZ was highlighted in a recent work on the effects of radiolysis on glass corrosion⁴³.

Experiment 2

To go further and address the aforementioned hypothesis, glass coupons recovered from the pH 9 experiment were corroded for an additional 43 days at pH 7 or 35 days at pH 5 and 3 (*Experiment 2*). More details are given in Supplementary Table 4. Because r_r increases with decreasing pH, changing the pH after the passivating gel has been formed will help identify the rate-limiting mechanisms. Figure 3a compares the response of the coupon re-corroded at pH 7 to that of a control sample (a coupon first corroded for 6 years at pH 7 and then corroded for another stage of 43 days at pH 7). Despite the fact that the two coupons do not have the same gel thickness, they corroded at the same rate: $0.12 \pm 0.02 \text{ nm d}^{-1}$ for the pH 9 sample and $0.11 \pm 0.02 \text{ nm d}^{-1}$ for the control sample. The control test is in line with *Experiment 1*, meaning that preparations for *Experiment 2* (rinsing, and immersion of the pre-corroded coupon in a fresh K-free solution within the short preparation period) did not affect the

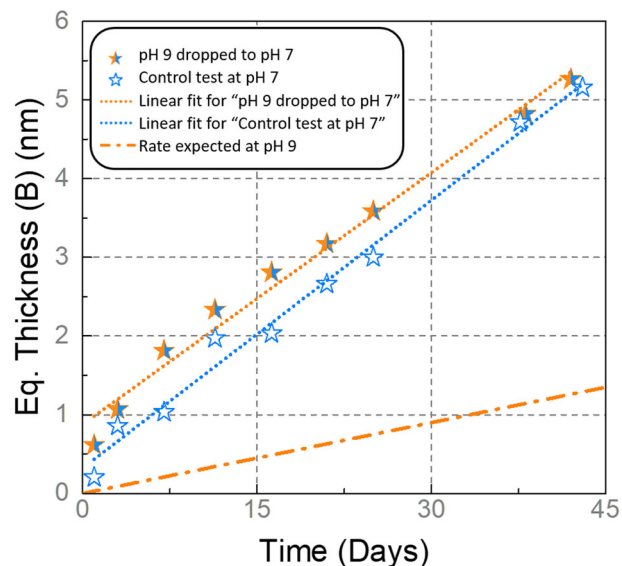


Fig. 3 Effect of a decrease in pH on ISG samples altered for 6 yr at pH 9. Equivalent thickness of altered glass calculated from B released during a 43-day immersion at pH 7, and comparison to a control test. B concentrations in *Experiment 2* are measured with a better accuracy than in *Experiment 1* because leachates are free of K and analyses are conducted by ICP-MS which offers a low detection limit.

glass response. Therefore, dropping the pH from 9 to 7 induces an acceleration of the rate by a factor of ~ 4 , with no detectable delay due to the presence of the passivating gel. Considering experimental uncertainties, this factor agrees with the difference in residual rates obtained at pH 7 and 9 (*Experiment 1*). It must be pointed out that this impact is only detectable from solution analysis. Indeed, the ToF-SIMS profiles of B before and after this second stage of corrosion at pH 7 are similar (Supplementary Fig. 4). According to solution data, the increase in gel thickness is only 5 nm after 43 days (Fig. 3a), which is less than 2% of the gel thickness formed at pH 9 and is thus too small to be detected by ToF-SIMS (Supplementary Fig. 4). In contrast, *Experiment 2* performed at pH 3 and 5 induced larger changes easily detectable by ToF-SIMS (Fig. 4b, c). These acid corrosion tests yielded extensive changes in the gel thickness and composition (see the difference with the reference sample, Fig. 4a). First, the gel thickness increased by 400 nm and 250 nm at pH 3 and pH 5, respectively. Second, the new gels formed in acid solutions were Na-depleted but retained large fractions of B and Ca, two elements known to be highly soluble in acid pH. Third, the part of the gels initially formed at pH 9 eventually retained more B and Ca than before the pH change. These last two observations indicate that the 3 mobile glass cations were dissolved at a higher rate due to the acid attack and that B and Ca were trapped in the passivating gel. To further confirm the quantification of B and Ca retention in the alteration layer by ToF-SIMS depth profiling, the sample re-corroded at pH 5 was also analyzed by X-ray photoelectron spectroscopy (XPS) (Supplementary Note 1, Supplementary Table 1, Supplementary Fig. 5). Good agreement was obtained between the two techniques.

The results of *Experiment 2* support the following mechanistic interpretation. Acid hydrous species (H^+ , H_3O^+) diffuse through the passivating gel formed at pH 9 and react with Na, B and Ca in the pristine glass, and Na diffuse out faster than B and Ca. The accumulation of B and Ca in the different parts of the gel can be explained by a lower diffusivity of $\text{B}_{(\text{aq})}$ and $\text{Ca}_{(\text{aq})}$ compared to hydrous species or by precipitation of Ca-borate phases. Geochemical calculations performed with the Chess code⁴⁴ show

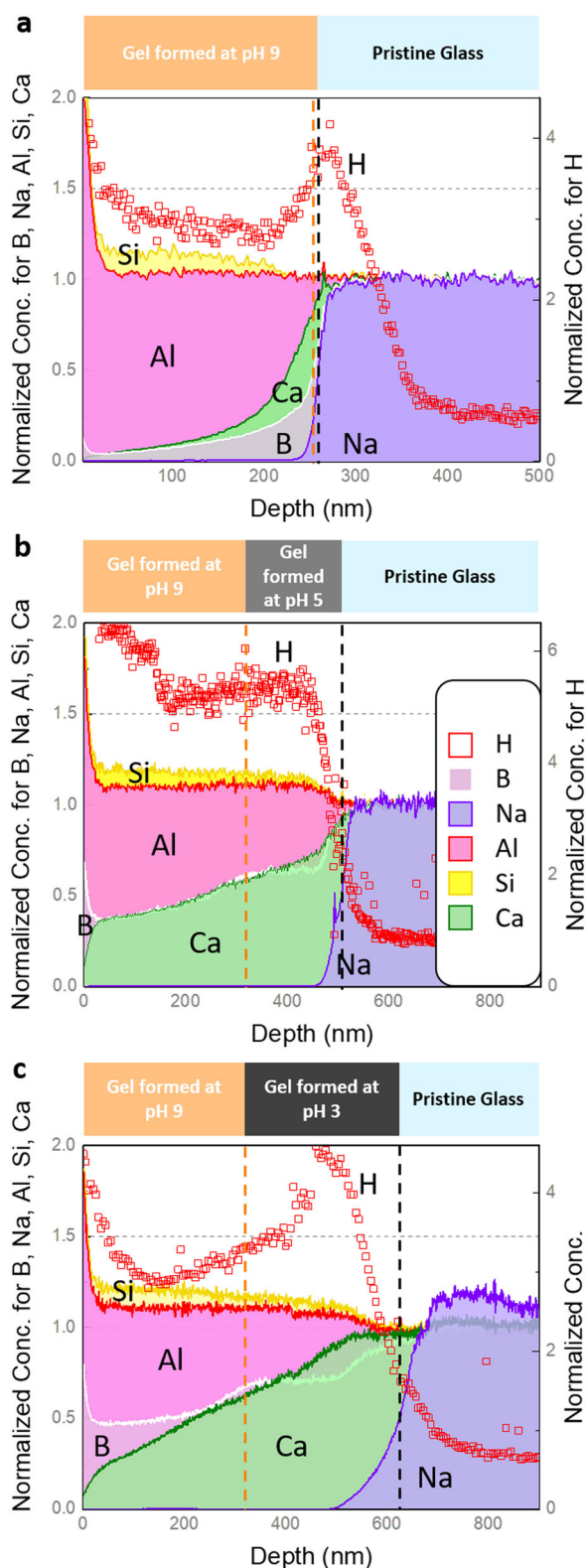


Fig. 4 Effect of a decrease in pH on ISG samples altered for 6 yr at pH 9. **Elemental ToF-SIMS profiles of glass cations and H.** **a** Before the pH swap. **b** After a 35-day immersion at pH 3. **c** Same as **b** but for the re-corrosion stage at pH 5. For **b** and **c** plots the orange dotted line indicates the position of the pristine glass surface before the pH swap. Therefore the gel located in between the orange and the black lines was formed during the stage of acid corrosion.

that precipitation of Ca-borate minerals seems unlikely below pH 6, but that precipitation of B hydroxide cannot be ruled out (Supplementary Note 2, Supplementary Table 2, Supplementary Fig. 6). Nonetheless, if nuclei form in pore water, they could partially or totally clog pores. Indeed, a previous study found that tracing molecules of 1 nm in size could not enter the passivating gel formed at pH 7²⁹. Collin et al also showed that the water content and mobility in those gels decreased in the presence of large alkali ions such as K⁺ or Cs⁺ in pores³⁶. Although more work is needed to identify the chemical speciation of B and Ca retained in the gel, the findings of this study demonstrate, for the first time, that a passivating gel can act as a trap for mobile glass species, especially B, which has extensively been used as a glass corrosion tracer. Consequently, the use of this element as a corrosion tracer should be considered cautiously.

To estimate the consequences of B and Ca retention in the gel on further glass corrosion, we performed a quick test consisting in placing a coupon of pristine ISG in a solution at pH~6.5, saturated with respect to SiO₂ and highly concentrated in B (~5 M), Ca (~2 M), and Na (~0.2 M), in order to mimic the mean concentrations recorded in the gels. After one day, the coupon was withdrawn, rinsed, dried and analyzed by ToF-SIMS. Supplementary Fig. 7 shows that around 5 nm of glass were corroded, whereas, according to *Experiment 1*, more than 200 nm of corroded glass were expected in the absence of B, Ca and Na. Although this single experiment provides preliminary results, it strongly suggests that high concentrations of B and Ca in the leachate reduce the rate of dissolution of B from the glass, and thus, by extrapolation, that the retention of B and Ca in the gel limits the extent of corrosion.

To summarize, the two first experiments of this study show that B release could be limited by several factors (hydrolysis, transport of hydrous species, transport of hydrolyzed species, and potentially precipitation within the gel) as is the case for Si. To better understand the links between the various mechanisms involving B and Si, and to lay the foundations for a model of the residual rate, the behavior of B in the absence of a passivating gel must be understood. ISG has a slightly larger number of B-O-Si linkages than Si-O-Si linkages⁴⁵, suggesting that B dissolution must strongly impact both the dissolution of the silicate network and the formation of the gel.

Experiment 3

To this end, parametric studies (*Experiment 3*) were conducted with pristine ISG samples corroded in controlled pH and temperature conditions with solutions pre-saturated with respect to amorphous silica in order to prevent silicate network dissolution. In all tested conditions, B was linearly released up to a few tens or hundreds of nm depending on the temperature, and the B release then followed a square-root-of-time dependency, likely because diffusion through the remnant Si-rich layer became limiting. A maximum rate, $r_m(B)$, was derived from the initial linear release and an apparent diffusion coefficient, D_B , was calculated according to the Fick's equation within the parabolic release regime (see the Methods section for details) (Supplementary Table 3, Supplementary Fig. 8). Figure 5a shows the maximum dissolution rate of B as a function of pH in silica-saturated solution (red circles) and compares it with that in dilute solution (blue circles) obtained by Inagaki et al.³⁵ In dilute solutions, $r_m(B)$ corresponds to the so-called initial or forward dissolution rate. In acid pH, the two datasets are comparable to each other meaning that the initial release of B is not impacted by the presence of dissolved silica. With increasing pH, $r_m(B)$ continuously diminishes, and beyond pH 6-7, it becomes lower than the dissolution rate of Si in dilute solutions (green circles). In the silica-saturated solution at basic pH, either the high condensation rate of Si-O-Si linkages⁴⁶ could impact the accessibility of B sites and thus could

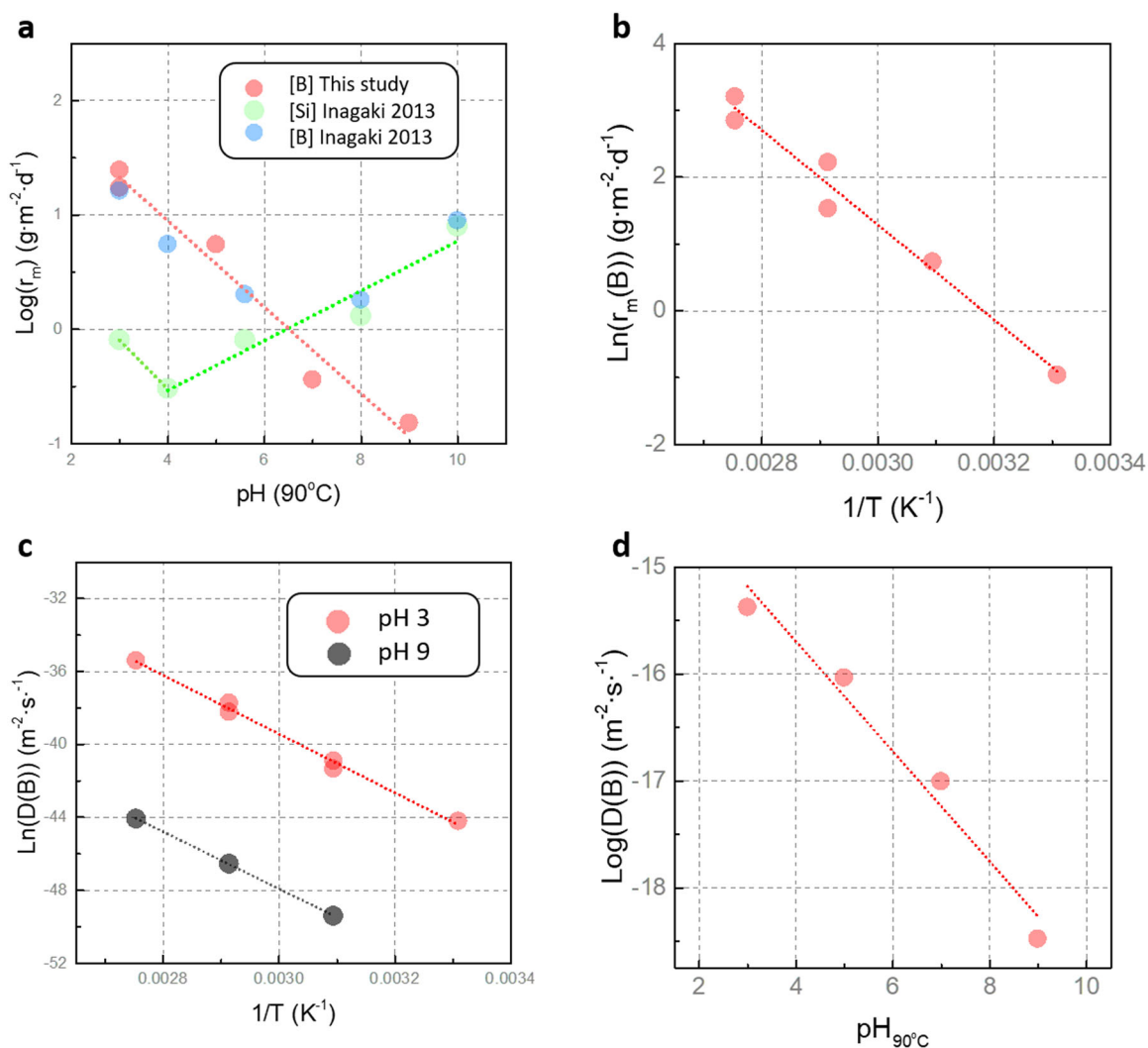


Fig. 5 pH and temperature effects on B release rate in Si-saturated solutions. **a** B dissolution rate in silica saturated solutions (red symbols) compared to literature data obtained far from saturation, i.e., in extremely dilute solutions ($\text{C}(\text{Si}) < 1 \text{ mg}\cdot\text{L}^{-1}$). Green (Si) and blue symbols (B) correspond to the so-called initial or forward dissolution rate, determined far from saturation. **b** Arrhenius plot for maximum dissolution rate of B, $r_m(\text{B})$, from experiments conducted at pH 3 in Si-saturated solutions. **c** Arrhenius plot for diffusion coefficient of B, $D(\text{B})$, from experiments conducted in Si-saturated solutions at pH 3 and pH 9. **d** Apparent diffusion coefficient of B, $D(\text{B})$, as a function of $\text{pH}_{90^\circ\text{C}}$ from experiments conducted at 90°C in Si-saturated solutions.

reduce the dissolution rate of B, or the intrinsic dissolution rate of Si–O–B linkages is reduced. This requires further investigations. Interestingly, the continuous and monotonic trend displayed by $r_m(\text{B})$ over a broad pH range may suggest that the same reaction could control B dissolution between pH 3 and 9. According to first principles simulations, this reaction implies the nucleophilic attack of H^+ on B and the hydrolysis of B–O–Si by H_2O ⁴⁷. The apparent activation energy for B release at pH 3 is $59 \pm 5 \text{ kJ mol}^{-1}$ (Fig. 5b), a value close but slightly lower than that for Si dissolution ($64 \pm 3 \text{ kJ mol}^{-1}$ from pH 3 to 5.6)³⁵. From the parabolic trend following the initial release of B, an apparent diffusion coefficient of B was calculated at 90°C (Fig. 5d):

$$D_B(\text{m}^2\text{s}^{-1}) = 10^{-13.65 - 0.51\text{pH}} \quad (2)$$

The corresponding activation energy at pH 3 is $60 \pm 6 \text{ kJ mol}^{-1}$ for the release rate of B in the parabolic regime, same as that associated to $r_m(\text{B})$. This leads to the conclusion that temperature has a negligible effect on the transport rate of reactants and reaction products through the growing Si-rich layer, as compared to the hydrolysis of B–O–Si linkages. In basic pH (pH 9), the activation energy for B release in the parabolic regime is same as

that determined at pH 3 (Fig. 5c). This result must be considered when further experiments will discuss the cause of the slow B release rate in silica saturated and basic solutions.

The results of *Experiment 3* can be used to estimate the gel thickness that would have formed during the second stage of *Experiment 2* (35 days at pH 3 or 5, and 42 days at pH 7) in the absence of a passivating gel. Application of Fick's law with the diffusion coefficients given by Eq. 2 gives a gel thickness of 50 μm , 15.5 μm , and 5 μm at pH 3, 5, and 7, respectively. Although these values are extrapolated from short-term data, the value at pH 3 is in fair agreement with results from a previous study (Supplementary Fig. 9)⁷. These values are 2 to 3 orders of magnitude higher than the thickness of actual gels formed during the second stage of *Experiment 2*. The most likely hypothesis to account for this difference is to consider that the gel formed at pH 9 reduced the flux of reactant species (H_2O , H_3O^+) reaching the AZ. This hypothesis was also supported by O isotopic tracing experiments with gels formed at pH 7²⁷ and by MD simulations³⁸. Interestingly, these simulations explain that the formation of small ring structures hindering water mobility within the gel is tied to medium range structures within the pristine glass.

DISCUSSION

To summarize, our experiments show that, in contrast to the commonly accepted notion of B as an ideal tracer of glass corrosion at any reaction progress, B can be retained in highly passivating gels. In such cases, Na seems to be a better tracer. More importantly, the findings of this work indicate that B dissolution in the so-called active zone limits the dissolution of all the soluble elements (i.e., Na and Ca in the case of ISG). In other words, if B–O–Si bonds are not broken, Na and Ca atoms in the vicinity of B cannot dissolve. This result suggests that B plays a greater role on glass durability than what thought before. In the present study, we demonstrated that the release rate of B in silica-saturated conditions, and by extension the residual rate, can be limited by three mechanisms: (i) the rate of hydrolysis of B–O–Si linkages, which has been parameterized as a function of pH and time for the diffusive regime; (ii) the inward diffusion of H^+ or H_3O^+ through the passivating gel; and (iii) the outward diffusion of aqueous B species through the passivating gel with potential precipitation in nanopores. Processes (i) and (ii) are dominating in *Experiment 1* and *Experiment 2* at pH 7, whereas process (iii) is key in *Experiment 2* at pH 3 and 5. All these three mechanisms are not independent and cannot be decoupled from the other mechanisms involving Si (Fig. 6). Indeed, ISG contains slightly more Si–O–B than Si–O–Si linkages and a very low number of B–O–B linkages⁴⁵.

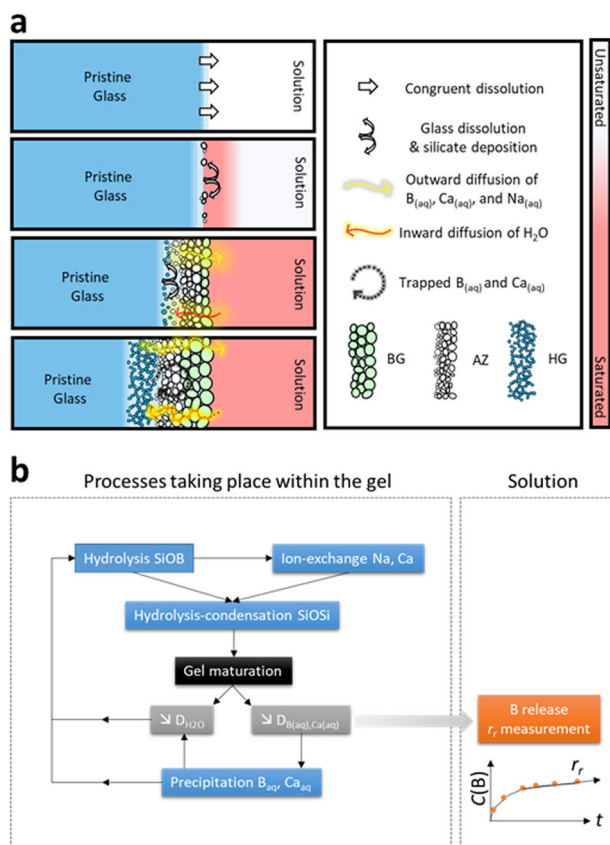


Fig. 6 Conceptualization of the mechanisms controlling the residual rate. **a** Schematic outline of the proposed glass corrosion model. The corrosion rate corresponds to derivate of the transformation of the pristine material into alteration products (dissolved species, gel, secondary minerals) with respect to time. The residual rate regime starts when Si-saturation of the contacting solution is achieved. The restructuring of the gel which eventually leads to the formation of a diffusion barrier for water and dissolves species is intimately tied to the release of mobile elements from the glass structure. **b** Interplay between the mechanisms involved in the residual rate regime.

As a result, when a B atom is dissolved, two silanol groups are formed and can condense to form a new siloxane bond. Multiple condensation reactions eventually affect the transport of aqueous species through the process of pore closure. Furthermore, if dissolved B and Ca from the active zone re-precipitate in nanopores, it can, in turn, reduce the inward diffusion of hydrous species. It is important to bear in mind that the gel network is a dynamic structure that evolves and matures owing to hydrolysis and condensation reactions involving Si. The current kinetic models, even those including passivation^{14,15,48}, do not ascribe any role to B, except that on the pH owing to the acid-basic properties of $B(OH)_3/B(OH)_4^-$. This relies on the assumption that B dissolution and transport are faster than the other mechanisms. Although this assumption is valid when far from saturation with respect to silica, it needs to be revised in the passivating regime. The findings in this study thus pave the way to a new model for glass corrosion (Fig. 6). The next step will be to implement the mechanisms reported in this article in a reactive transport code with a discretization of the alteration layer to account for the various steps of glass corrosion when a pristine glass is placed in contact with water:

- Congruent dissolution of the glass elements in neutral and basic pH conditions, or incongruent dissolution in acid pH conditions, until silica-saturated conditions are achieved
- Beyond saturation, further dissolution of B until significant amount of pores are closed within the gel. Parameterization of B dissolution is given in this article. Ca and Na dissolution is imposed by that of B. To a first approximation, a first-order rate law including an affinity term can be used to describe the pseudo-equilibrium between the Si-rich passivating layer and the bulk solution.
- Reduction of water diffusion depending on the fraction of remaining open pores in the passivating layer.
- Reduction of $B_{(aq)}$ and $Ca_{(aq)}$ diffusion depending on the fraction of remaining open pores in the passivating layer.
- Reduction of B dissolution rate at the glass interface according to the local concentration of $B_{(aq)}$ and $Ca_{(aq)}$. This would enable the precipitation of borate minerals in the pores with potential consequences on the transport of water molecules. This part requires more parametric studies.

There is still a lack of understanding to correlate porosity of the gel with the diffusivity of aqueous species. Molecular dynamics and Monte Carlo simulations are promising means to decipher the structure and properties of nanoporous networks^{20,49–51}, but more work is needed to parameterize laws for reactive transport models. Furthermore, although we have focused on a simple glass that does not form secondary silicate minerals, borosilicate nuclear waste glasses are known to form phyllosilicates, calcium silicate hydrates, and/or zeolites as corrosion products^{52–56}. The precipitation of these minerals disrupts the passivating layer^{57–59}. This type of mechanism is already implemented in reactive transport codes, but with no retroaction on the transport properties of the gel⁶⁰. Furthermore, passivation is generally described by an apparent diffusion coefficient applicable to one or all species⁶⁰. Beyond the development of mechanistic models, the results of this study provide clues to determine the most favorable geochemical environment to guarantee the safety of geological disposals of nuclear wastes.

METHODS

Materials

ISG (60.2 SiO₂, 16.0 B₂O₃, 12.6 Na₂O, 5.7 CaO, 3.8 Al₂O₃, and 1.7 ZrO₂ in mol %) was produced in 2012 by MoSci Corporation (Rolla, MO, USA) and has been served since then as a reference material for glass corrosion studies^{28,61}.

Leaching experiments

Experiment 1 is described in details in previous articles^{27,29,30}. It consisted of two batch of experiments conducted at 90 °C, fixed pH90 °C (7 or 9) with glass coupons corroded in a solution initially close to saturation with respect to amorphous $^{29}\text{SiO}_2$ ($C_0(\text{Si}) = 141 \text{ mg L}^{-1}$ at $\text{pH}_{90^\circ\text{C}} 7$ and $C_0(\text{Si}) = 275 \text{ mg L}^{-1}$ at $\text{pH}_{90^\circ\text{C}} 9$). Unless otherwise specified, all pH values were measured at 90 °C in this study. The solutions also contained a large amount of K, an element used to dissolve $^{29}\text{SiO}_2$, which eventually contributed to improving passivation properties of the gel³⁶. At various time durations, solution samples or coupons were taken for analysis. In *Experiment 2*, glass coupons altered for 2312 days in *Experiment 1* were taken out of the leaching solution, rinsed quickly with deionized water, then immersed in a fresh solution for a second short stage of corrosion at a different pH. This second stage of corrosion was conducted at 90 °C, in solution saturated with respect to amorphous $^{28}\text{SiO}_2$, with no addition of K and at fixed pH90 °C of 3, 5, 7, or 9. The experimental matrix is given in Supplementary Table 4. Solution samples taken during the second stage were analyzed by ICP-MS and 2 coupons were characterized at the end of *Experiment 2* by ToF-SIMS. *Experiment 3* consisted of a series of parametric tests conducted with pristine ISG samples corroded at various temperatures (30, 50, 70, and 90 °C) and pHs (3, 5, 7, and 9). The tests were designed to measure the initial release rate of B when silica saturated conditions are achieved but before the gel becomes passivating. Therefore, all the tests in these series were conducted in solution saturated with respect to amorphous $^{28}\text{SiO}_2$. Polished glass monoliths or glass powder (63–125 μm) with a specific surface area of $535 \text{ cm}^2\text{g}^{-1}$, as determined by the Brunauer Emmett and Teller (BET) method were employed for these short duration tests (from a few hours to a few days). Solution samples were taken at regular intervals and were analyzed by UV-visible spectrophotometry.

Solution analysis

The solutions from *Experiment 1* were diluted by a factor 10–30 to lower the concentration of K and were analyzed by inductively coupled plasma-optical emission spectroscopy (Thermo Scientific, ICAP 6300 DUO). Because of the high dilution, B concentrations were slightly above detection limit (0.05 mg L^{-1}). A relative uncertainty of 10% was considered. The solutions from *Experiment 2* were analyzed by inductively coupled plasma-mass spectrometry (Thermo Scientific, ICAP Q). Continuous monitoring of cleanliness of the analysis device, adjustment of calibration to the measured concentrations and dilution adapted to the low volume of solutions supplied and all elements present in the matrix, made it possible to obtain a detection limit for B of ~ 1 ppb with relative uncertainty of 10%. Solution from *Experiment 3* were analyzed by colorimetry with a Merck Spectroquant kit and a Cary Varian UV-visible spectrophotometer at a wavelength of 405 nm (concentration range: $0.05\text{--}2 \text{ mg L}^{-1}$, error 5%). For each tested condition, B release was initially linear and then became parabolic. The initial linear portion of the B curve was used to determine the maximum dissolution rate of B, $r_m(\text{B})$, and the parabolic portion of the curve was used to determine the diffusion coefficient of B through the remaining Si-rich layer, $D(\text{B})$. $r_m(\text{B})$ was calculated as follow:

$$r_m(\text{B}) = \frac{d}{dt}(NL(\text{B})) = \frac{d}{dt}\left(\frac{C(\text{B})}{\frac{S}{V}x_B}\right) \quad (3)$$

where $NL(\text{B})$ is the normalized mass loss of the glass calculated from B, $C(\text{B})$ is the concentration of B in the solution, S/V is the glass-surface-area-to-solution-volume ratio, and x_B the mass fraction of B in the glass. $D(\text{B})$ was calculated from the following formula which results from the application of the second Fick's law to a semi-infinite diffusion medium²²:

$$\frac{NL(\text{B})}{\rho} = 2\sqrt{\frac{D(\text{B})t}{\pi}} \quad (4)$$

where ρ is the glass density (2.5 g cm^{-3}). Uncertainties on $r_m(\text{B})$ and $D(\text{B})$ were $\pm 30\%$ and $[-50\%, +100\%]$, respectively. Note that in *Experiment 1*, where it was previously demonstrated that the gel results from an isovolumetric process (gel thickness = thickness of altered glass), and that the retention factor of B in the gel is low, $\frac{NL(\text{B})}{\rho}$ gives a good estimation of the gel thickness.

Time-of-Flight Secondary Ion Mass Spectrometry (ToF-SIMS) analysis

ToF-SIMS analyses were performed by Tescan Analytics, Fuveau, France using a ToF-SIMS5 spectrometer (IonToF—Münster, Germany). The

following conditions were applied: sputter beam of 1.0 keV, 300 nA O_2^+ , abraded area of $200 \times 200 \mu\text{m}^2$, analysis beam of 25.0 keV, 0.2 pA Bi^+ , analyzed area of $60 \times 60 \mu\text{m}^2$, charges compensated by an electron gun. Data acquisition and post-processing analyses were performed using the SurfaceLab 6 software. A profilometer was used to measure the crater depth at the end of the analysis. Data are normalized to Zr, an immobile element in the gel, and displayed as a function of depth considering the same sputtering rate in the alteration layer and pristine glass. More details are given in recent articles^{29,30,62}.

DATA AVAILABILITY

The data that support the findings of this study are available from the corresponding authors on reasonable request.

Received: 31 August 2020; Accepted: 18 November 2020;

Published online: 11 December 2020

REFERENCES

- Ojovan, M. I., Lee, W. E. & Kalmykov, S. N. *An introduction to nuclear waste immobilisation*. 3rd edn, (Elsevier, 2019).
- Guo, X. L. et al. Self-accelerated corrosion of nuclear waste forms at material interfaces. *Nat. Mater.* **19**, 310–316 (2020).
- Gin, S., Jollivet, P., Tribet, M., Peugeot, S. & Schuller, S. Radionuclides containment in nuclear glasses: an overview. *Radiochim. Acta* **105**, 927–959 (2017).
- Mallants, D., Marivoet, J. & Sillen, X. Performance assessment of the disposal of vitrified high-level waste in a clay layer. *J. Nucl. Mater.* **298**, 125–135 (2001).
- Frankel, G. S. et al. A comparative review of the aqueous corrosion of glasses, crystalline ceramics, and metals. *npj Mater. Degrad.* **2**, 15 (2018).
- Jollivet, P. et al. Effect of clayey groundwater on the dissolution rate of the simulated nuclear waste glass SON68. *J. Nucl. Mater.* **420**, 508–518 (2012).
- Fournier, M. et al. Effect of pH on the stability of passivating gel layers formed on International Simple Glass. *J. Nucl. Mater.* **524**, 21–38 (2019).
- Gin, S. In *2nd International Summer School on Nuclear Glass Wasteform: Structure, Properties and Long-Term Behavior*. Vol. 7 *Procedia Materials Science* (eds et al.) 163–171 (Elsevier Science Bv, 2014).
- Vienna, J. D., Ryan, J. V., Gin, S. & Inagaki, Y. Current understanding and remaining challenges in modeling long-term degradation of borosilicate nuclear waste glasses. *Int. J. Appl. Glass Sci.* **4**, 283–294 (2013).
- Grambow, B. in *MRS Proceedings.02/26* edn 15 (Cambridge University Press).
- Aagaard, P. & Helgeson, H. C. Thermodynamic and kinetic constraints on reaction-rates among minerals and aqueous-solutions. 1. Theoretical considerations. *Am. J. Sci.* **282**, 237–285 (1982).
- Gin, S., Jegou, C., Frugier, P. & Minet, Y. Theoretical consideration on the application of the Aagaard-Helgeson rate law to the dissolution of silicate minerals and glasses. *Chem. Geol.* **255**, 14–24 (2008).
- Delage, F., Ghaleb, D., Dussossoy, J. L., Chevallier, O. & Vernaz, E. A mechanistic model for understanding nuclear waste glass dissolution. *J. Nucl. Mater.* **190**, 191–197 (1992).
- Frugier, P. et al. SON68 nuclear glass dissolution kinetics: current state of knowledge and basis of the new GRAAL model. *J. Nucl. Mater.* **380**, 8–21 (2008).
- Grambow, B. & Muller, R. First-order dissolution rate law and the role of surface layers in glass performance assessment. *J. Nucl. Mater.* **298**, 112–124 (2001).
- Advocat, T., Crovisier, J. L., Fritz, B. & Vernaz, E. *Thermokinetic Model Of Borosilicate Glass Dissolution - Contextual Affinity*. Vol. 176 (Materials Research Soc, 1990).
- Munier, I., Crovisier, J. L., Grambow, B., Fritz, B. & Clement, A. Modelling the alteration gel composition of simplified borosilicate glasses by precipitation of an ideal solid solution in equilibrium with the leachant. *J. Nucl. Mater.* **324**, 97–115 (2004).
- Bourcier, W. L., Peiffer, D. W., Knauss, K. G., McKeegan, K. D. & Smith, D. K. A kinetic-model for borosilicate glass dissolution based on the dissolution affinity of a surface alteration layer. Vol. 176 (Materials Research Soc, 1990).
- Ebert, W. L. & Jerden, J. L. Parameterizing a borosilicate waste glass degradation model. *npj Mater. Degrad.* **3**, 31 (2019).
- Pierce, E. M., Frugier, P., Criscenti, L. J., Kwon, K. D. & Kerisit, S. N. Modeling interfacial glass-water reactions: recent advances and current limitations. *Int. J. Appl. Glass Sci.* **5**, 421–435 (2014).
- Gin, S. in *Scientific Basis for Nuclear Waste Management Xxiv*. Vol. 663 *Materials Research Society Symposium Proceedings* (eds K. P. Hart & G. R. Lumpkin) 207–215 (Materials Research Society, 2000).
- Chave, T., Frugier, P., Ayrat, A. & Gin, S. Solid state diffusion during nuclear glass residual alteration in solution. *J. Nucl. Mater.* **362**, 466–473 (2007).

23. Goût, T. L. et al. Diffusive processes in aqueous glass dissolution. *npj Mater. Degrad.* **3**, 39 (2019).
24. Ferrand, K., Abdelouas, A. & Grambow, B. Water diffusion in the simulated French nuclear waste glass SON 68 contacting silica rich solutions: experimental and modeling. *J. Nucl. Mater.* **355**, 54–67 (2006).
25. Ojovan, M. I., Pankov, A. & Lee, W. E. The ion exchange phase in corrosion of nuclear waste glasses. *J. Nucl. Mater.* **358**, 57–68 (2006).
26. Frugier, P., Gin, S., Lartigue, J. E. & Deloué, E. In *Scientific Basis for Nuclear Waste Management XXIX* Vol. 932 *Materials Research Society Symposium Proceedings* (ed P. Vanlsegem) 305–+ (Materials Research Soc, 2006).
27. Gin, S. et al. Dynamics of self-reorganization explains passivation of silicate glasses. *Nat. Commun.* **9**, 9 (2018).
28. Gin, S. et al. An international initiative on long-term behavior of high-level nuclear waste glass. *Mater. Today* **16**, 243–248 (2013).
29. Gin, S. et al. Origin and consequences of silicate glass passivation by surface layers. *Nat. Commun.* **6**, 8 (2015).
30. Gin, S. et al. Atom-Probe Tomography, TEM and ToF-SIMS study of borosilicate glass alteration rim: a multiscale approach to investigating rate-limiting mechanisms. *Geochim. Cosmochim. Acta* **202**, 57–76 (2017).
31. Ngo, D. et al. Spectroscopic ellipsometry study of thickness and porosity of the alteration layer formed on international simple glass surface in aqueous corrosion conditions. *npj Mater. Degrad.* **2**, 20 (2018).
32. Collin, M. et al. Structure of International Simple Glass and properties of passivating layer formed in circumneutral pH conditions. *npj Mater. Degrad.* **2**, 4 (2018).
33. Kaya, H., Ngo, D., Gin, S. & Kim, S. H. Spectral changes in Si-O-Si stretching band of porous glass network upon ingress of water. *J. Non-Cryst. Solids* **527**, 6 (2020).
34. Gin, S. et al. The fate of silicon during glass corrosion under alkaline conditions: a mechanistic and kinetic study with the International Simple Glass. *Geochim. Cosmochim. Acta* **151**, 68–85 (2015).
35. Inagaki, Y., Kikunaga, T., Idemitsu, K. & Arima, T. Initial dissolution rate of the international simple glass as a function of pH and temperature measured using microchannel flow-through test method. *Int. J. Appl. Glass Sci.* **4**, 317–327 (2013).
36. Collin, M., Fournier, M., Charpentier, T., Moskura, M. & Gin, S. Impact of alkali on the passivation of silicate glass. *npj Mater. Degrad.* **2**, 16 (2018).
37. Cailleteau, C. et al. Insight into silicate-glass corrosion mechanisms. *Nat. Mater.* **7**, 978–983 (2008).
38. Du, T. et al. Atomistic origin of the passivation effect in hydrated silicate glasses. *npj Mater. Degrad.* **3**, 6 (2019).
39. Gin, S., Beaudoux, X., Angeli, F., Jegou, C. & Godon, N. Effect of composition on the short-term and long-term dissolution rates of ten borosilicate glasses of increasing complexity from 3 to 30 oxides. *J. Non-Cryst. Solids* **358**, 2559–2570 (2012).
40. Ducasse, T. et al. Alteration of synthetic basaltic glass in silica saturated conditions: analogy with nuclear glass. *Appl. Geochem.* **97**, 19–31 (2018).
41. Hellmann, R. et al. Nanometre-scale evidence for interfacial dissolution-precipitation control of silicate glass corrosion. *Nat. Mater.* **14**, 307–311 (2015).
42. Lanford, W. A. et al. Hydration of soda-lime glass. *J. Non-Cryst. Solids* **33**, 249–266 (1979).
43. Tribet, M. et al. New insights about the importance of the alteration layer/glass interface. *J. Phys. Chem. C* **124**, 10032–10044 (2020).
44. van der Lee, J., De Windt, L., Lagneau, V. & Goblet, P. Module-oriented modeling of reactive transport with HYTEC. *Comput. Geosci.* **29**, 265–275 (2003).
45. Lu, X. N., Ren, M. G., Deng, L., Benmore, C. J. & Du, J. C. Structural features of ISG borosilicate nuclear waste glasses revealed from high-energy X-ray diffraction and molecular dynamics simulations. *J. Nucl. Mater.* **515**, 284–293 (2019).
46. Nangia, S. & Garrison, B. J. Ab initio study of dissolution and precipitation reactions from the edge, kink, and terrace sites of quartz as a function of pH. *Mol. Phys.* **107**, 831–843 (2009).
47. Zapol, P., He, H. Y., Kwon, K. D. & Criscenti, L. J. First-principles study of hydrolysis reaction barriers in a sodium borosilicate glass. *Int. J. Appl. Glass Sci.* **4**, 395–407 (2013).
48. Grambow, B. A general rate equation for nuclear waste glass corrosion. *MRS Proc.* **44**, 15 (2011).
49. Perea, D. E. et al. Tomographic mapping of the nanoscale water-filled pore structure in corroded borosilicate glass. *npj Mater. Degrad.* **4**, 8 (2020).
50. Cailleteau, C., Devreux, F., Spalla, O., Angeli, F. & Gin, S. Why do certain glasses with a high dissolution rate undergo a low degree of corrosion? *J. Phys. Chem. C* **115**, 5846–5855 (2011).
51. Kerisit, S. & Du, J. C. Monte Carlo simulation of borosilicate glass dissolution using molecular dynamics-generated glass structures. *J. Non-Cryst. Solids* **522**, 7 (2019).
52. Mir, A. H. et al. Effect of decades of corrosion on the microstructure of altered glasses and their radiation stability. *npj Mater. Degrad.* **4**, 11 (2020).
53. Mann, C. et al. Influence of young cement water on the corrosion of the International Simple Glass. *npj Mater. Degrad.* **3**, 5 (2019).
54. De Echave, T. et al. Effect of clayey groundwater on the dissolution rate of SON68 simulated nuclear waste glass at 70 degrees C. *J. Nucl. Mater.* **503**, 279–289 (2018).
55. Curti, E., Crovisier, J. L., Morvan, G. & Karpoff, A. M. Long-term corrosion of two nuclear waste reference glasses (MW and SON68): a kinetic and mineral alteration study. *Appl. Geochem.* **21**, 1152–1168 (2006).
56. Backhouse, D. J. et al. Corrosion of the International Simple Glass under acidic to hyperalkaline conditions. *npj Mater. Degrad.* **2**, 29 (2018).
57. Ryan, J. V. et al. In-situ monitoring of seeded and unseeded stage III corrosion using Raman spectroscopy. *npj Mater. Degrad.* **3**, 34 (2019).
58. Fournier, M., Gin, S. & Frugier, P. Resumption of nuclear glass alteration: state of the art. *J. Nucl. Mater.* **448**, 348–363 (2014).
59. Gin, S., Frugier, P., Jollivet, P., Bruguier, F. & Curti, E. New insight into the residual rate of borosilicate glasses: effect of S/V and glass composition. *Int. J. Appl. Glass Sci.* **4**, 371–382 (2013).
60. Frugier, P., Minet, Y., Rajmohan, N., Godon, N. & Gin, S. Modeling glass corrosion with GRAAL. *npj Mater. Degrad.* **2**, 35 (2018).
61. Kaspar, T. C. et al. Physical and optical properties of the International Simple Glass. *npj Mater. Degrad.* **3**, 15 (2019).
62. Collin, M. et al. ToF-SIMS depth profiling of altered glass. *npj Mater. Degrad.* **3**, 14 (2019).

ACKNOWLEDGEMENTS

This work was supported as part of the Center for Performance and Design of Nuclear Waste Forms and Containers, an Energy Frontier Research Center funded by the U.S. Department of Energy, Office of Science, Basic Energy Sciences under Award # DESC0016584. We grateful to Elodie Chauvet and Yves De Puydt (Tescan Analytics) for the ToF-SIMS analyses, Géraldine Parisot (CEA) for the ICP-OES analyses, and Dr. Corkhill from Sheffield University and Dr. Inagaki from Kyushu University for fruitful discussions.

AUTHOR CONTRIBUTIONS

S.G. and J.M.D. designed the research; S.G. and K.D. performed the experiments; V.T. performed the ICP-MS analyses. S.G., X.G., J.M.D., F.A., J.D., S.K., and S.H.K. analyzed the data. All authors contributed to editing the manuscript, and approve of the content in its current form.

COMPETING INTERESTS

The authors declare no competing interests.

ADDITIONAL INFORMATION

Supplementary information is available for this paper at <https://doi.org/10.1038/s41529-020-00145-2>.

Correspondence and requests for materials should be addressed to S.G.

Reprints and permission information is available at <http://www.nature.com/reprints>

Publisher's note Springer Nature remains neutral with regard to jurisdictional claims in published maps and institutional affiliations.



Open Access This article is licensed under a Creative Commons Attribution 4.0 International License, which permits use, sharing, adaptation, distribution and reproduction in any medium or format, as long as you give appropriate credit to the original author(s) and the source, provide a link to the Creative Commons license, and indicate if changes were made. The images or other third party material in this article are included in the article's Creative Commons license, unless indicated otherwise in a credit line to the material. If material is not included in the article's Creative Commons license and your intended use is not permitted by statutory regulation or exceeds the permitted use, you will need to obtain permission directly from the copyright holder. To view a copy of this license, visit <http://creativecommons.org/licenses/by/4.0/>.